

# Prototype Testing for a Copper Rotatable Collimator for the LHC Collimation Upgrade\*

Jeffrey Claiborne Smith<sup>†</sup>, Gene Anzalone, Eric Doyle, Lewis Keller,  
Steven Lundgren, Thomas Walter Markiewicz, Reggie Rogers  
(SLAC National Accelerator Laboratory, Menlo Park, California)

December, 2008

## Abstract

The Phase II upgrade to the LHC collimation system calls for complementing the robust Phase I graphite collimators with high Z Phase II collimators. The design for the collimation upgrade has not been finalized. One option is to use metallic rotatable collimators and testing of this design will be discussed here.

The Phase II collimators must be robust in various operating conditions and accident scenarios. A prototype collimator jaw referred to as RC0 has been tested for both mechanical and thermal compliance with the design goals. Thermal expansion bench-top tests are compared to ANSYS simulation results.

The prototype has also been tested in vacuum bake-out to confirm compliance with the LHC vacuum spec. CMM equipment has been used to verify the flatness of the jaw surface after heat tests and bake-out.

## 1 INTRODUCTION

The principle function of LHC collimation system is to protect the superconducting magnets from quenching due to particle losses. The collimation system must absorb upwards of 90 kW in the steady state operating condition (1 hr beam lifetime) and withstand transient periods where up to 450 kW is deposited for no more than 10 seconds. The maximum energy deposited on any one secondary collimator is 23 kW for the steady state and 115 kW for the transient condition [1]. The system must also be robust against an accident scenario where up to 8 full intensity bunches impact on one collimator jaw due to an asynchronous firing of the beam abort system imparting 1 MJ over 200 ns [2]. In the steady state condition the maximum heat deformation of the jaw toward the beam should be no more than 25 microns relative to the  $7\sigma$  initial aperture. When fully inserted the minimum half gap is 0.5 mm which corresponds to 7 sigma. The jaws must also move in parallel  $\pm 5$  mm back and forth

---

\*Work supported in part by the U.S. Department of Energy contract DE-AC02-76SF00515

<sup>†</sup>js344@slac.stanford.edu

at full insertion in order to follow the beam centroid. Additionally, when the jaws are fully retracted, the minimum aperture must be 45 mm.

For the phase I collimation system, it was decided to use graphite, a low Z material, which can withstand the accident scenario with no damage. But due to the same low Z properties, the graphite collimators cannot absorb enough beam halo for the LHC to operate at design beam intensities. The plan is to upgrade the phase I collimators with up to 30 high Z phase II collimators. The high Z material of the phase II collimators will not withstand the impact of the 8 full intensity bunches in the accident scenario without permanent damage, so a rotatable jaw has been designed which will be recoverable. Composed of two cylindrical jaws, if a beam happens to hit a jaw it can be rotated to introduce a clean surface for continued operation. Over the course of the lifetime of the LHC it is estimated that any one collimator will experience the accident scenario no more than 20 times, so 20 flat facets on the cylindrical jaw surface is sufficient.

## 2 MECHANICAL DESIGN

The most critical issue in the design of the collimator is the thermal deflection of the jaws due to beam heat load. A variety of materials were investigated to determine which had the appropriate thermal and Z properties to sufficiently absorb the beam yet not rise above the melting point. Ultimately, copper was chosen as a balance between collimation efficiency, thermal deflection and manufacturability [3].

Each jaw consists of a molybdenum shaft and concentric glidcop jaw joined only at the center via a glidcop hub as illustrated in figure 1. This layout was dubbed the Jaw-Hub-Shaft concept. Between the shaft and outer jaw is a 2mm gap. This allows the jaw ends to deflect mostly away from the beam during heating, reducing the jaw deflection toward the beam. The use of molybdenum for the central shaft is to increase structural rigidity. The heat load on the central shaft is minimal so good thermal conductivity between it and the cooling coils in the jaw is not an issue.

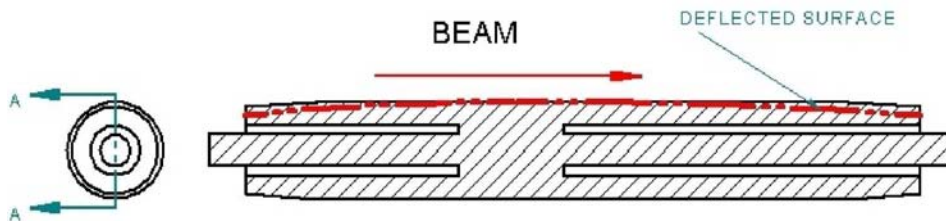


Figure 1: Jaw-Hub-Shaft concept to minimize the jaw deflection toward the beam.

The jaw must be water cooled. This introduces an obstacle to the rotation of the jaws. Any type of sliding seal was deemed impractical so instead a single long copper tube of length 16m is formed in a helix within the jaw, with straight tails extending through the center of the shaft. This eliminates any vacuum to water joints and allows for the copper tube to be twisted as the jaw rotates. The final jaw design is illustrated in figure 2 showing the inner

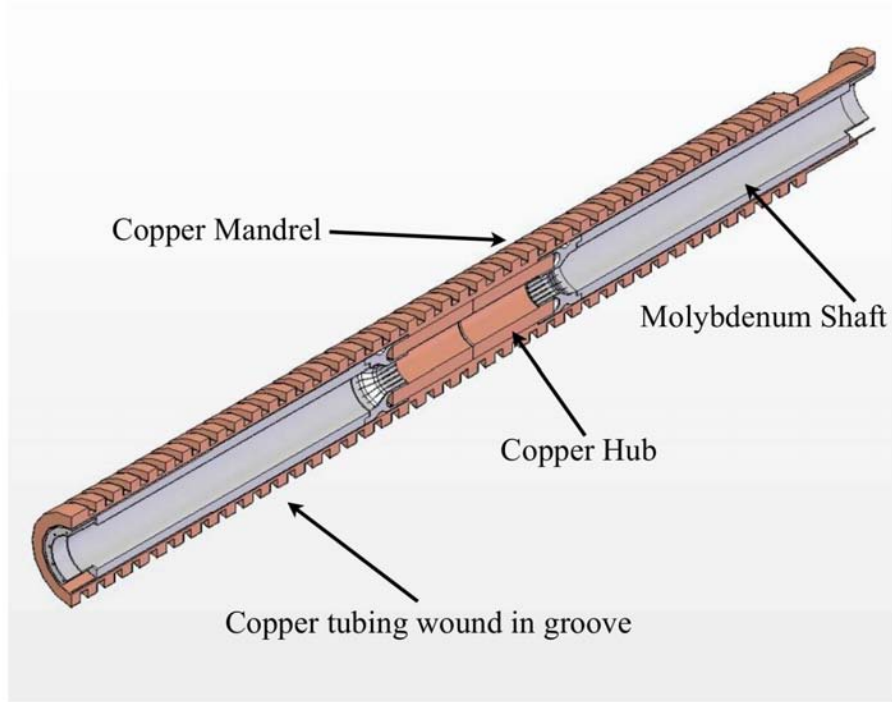


Figure 2: Cutaway of jaw showing inner molybdenum shaft and mandrel.

shaft and mandrel and figure 3 with the jaw surfaces added. The overall Jaw specifications are given in table 1

Table 1: Jaw Dimensions

Component	dimension	units
Jaw OD tangent to facet faces	136	mm
Jaw number of facets	20	
Jaw ID	66	mm
Jaw length, including edge taper	930	mm
Mo Shaft OD	64	mm
Mo Shaft ID	44	mm
Cooling tube ODxID (square)	10x7	mm
Embedded helix - center radius	80	mm
Helix - number of turns	47	
Total cooling tube length	16	m
Flow per jaw	9	l/min
Water velocity	3	m/s

An internally actuated drive has been designed that utilizes a ratchet attached to a “Geneva Mechanism,” or “Maltese Cross,” which translates a continuous rotation into an intermittent rotary motion, allowing for the precise rotation of the jaw in increments of 1/20th of a revolution, or one facet face. The mechanism effectively guarantees against the

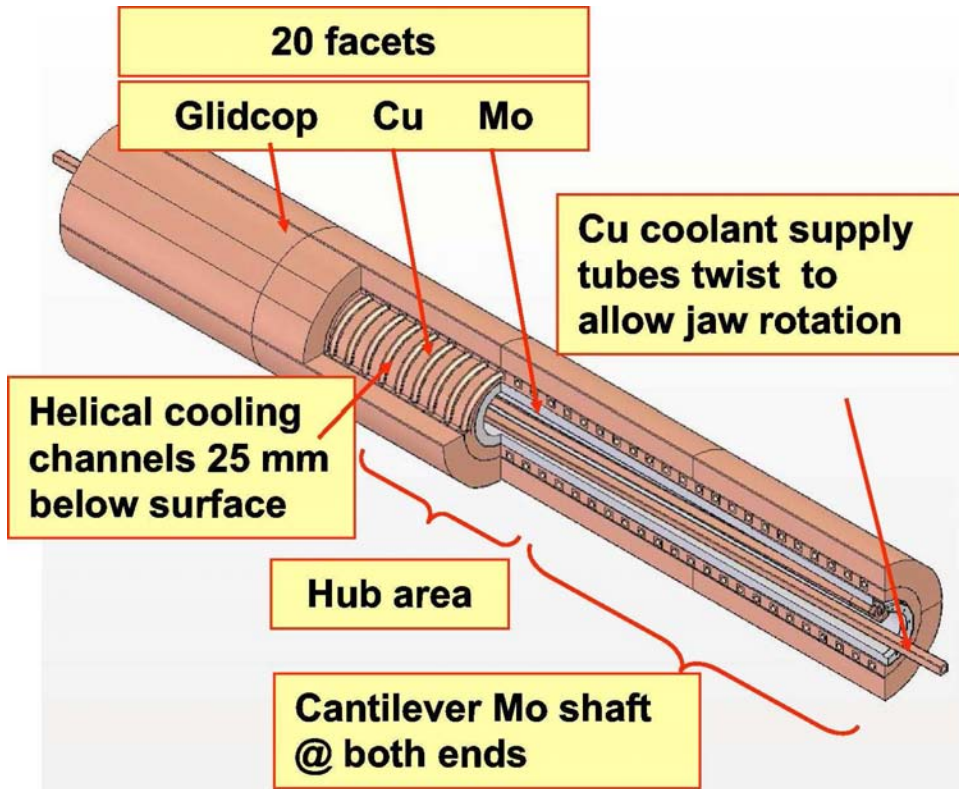


Figure 3: Cutaway of Jaw showing outer jaw surfaces and cooling tube routed through the center of the molybdenum shaft.

accidental over-rotating of the jaw because the jaw only begins to rotate after the 8th ratchet past the last rotation. The ratcheting is performed by over-retracting the jaw whereby the ratchet hits a “hammer” attached to the chamber wall. Successive over-retracting rotates the jaw with a total of 512 ratchets resulting in one facet rotation when using a tri-lobed geneva driver. The jaw shaft is supported on each end by a flexible molybdenum support which allows for jaw deflection due to gravity sag, thermal load and a skewed jaw orientation. The shaft support is shown in figure 4.

The mechanism for positioning the jaw in the beam path is to be adapted from the LHC Phase I Collimator design [2]. Given the heavier jaws in the rotatable jaw, modifications may be needed to the mechanism to support the greater weight. A phase I graphite collimator assembly has been obtained from CERN and is being used for designing the mechanism in the Phase II design. We expect to have to make only small changes to accept our heavier and larger jaws.

The overall design is illustrated in figure 5. The circular vacuum chamber was deemed the easiest and most robust chamber to construct. Additionally, current trapped modes studies have found this configuration to be ideal. The design concerns, measurements and simulations related to RF shielding have been discussed in a previous paper [4] but more studies are to continue with the current design.

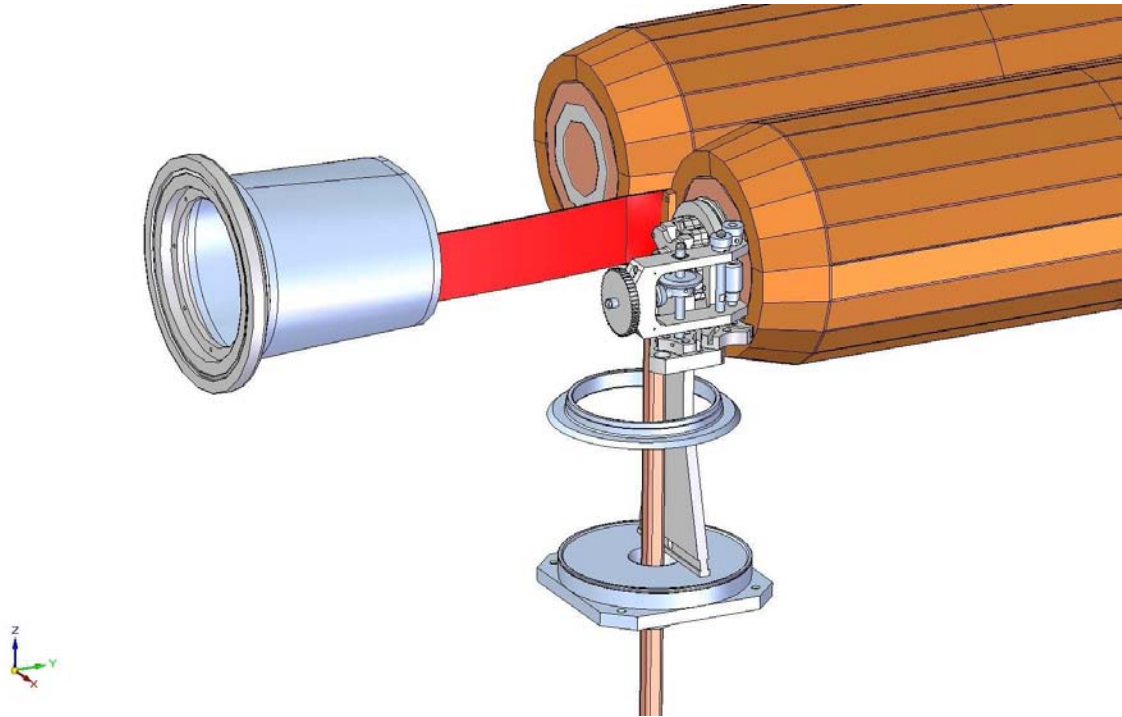


Figure 4: View of the shaft support showing the Geneva Mechanism for precision jaw rotation, flexible molybdenum shaft and image current foil.

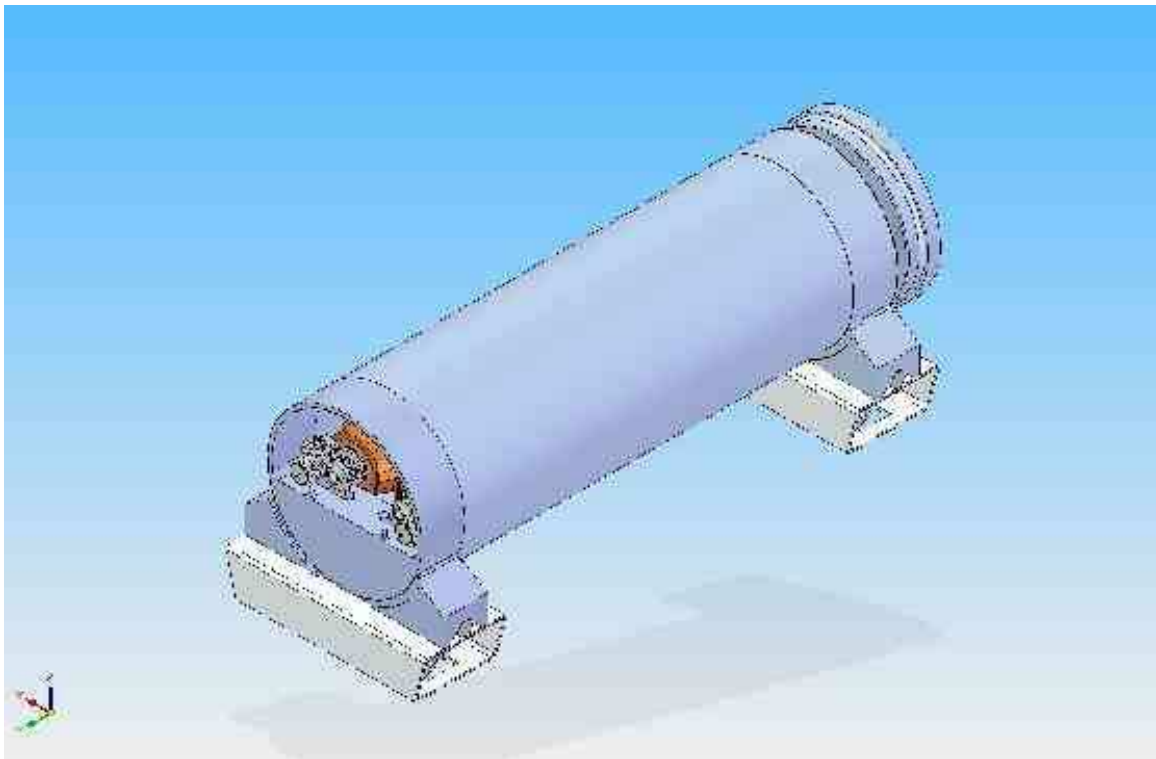


Figure 5: Full layout of the rotatable collimator the end flanges (not shown) are quickly removable for easy access.

### 3 PROTOTYPE CONSTRUCTION

Extensive R&D went into the design and fabrication of the first jaw prototype. Numerous braze joint tests were performed until a satisfactory method was developed. In particular, the joint attaching the molybdenum shafts to the central glidcop hub proved to be rather troublesome, mainly due to the different thermal expansions of glidcop and molybdenum. The solution was found by cutting fingers along the end of the molybdenum shaft as can be seen in figure 2. This setup allowed for the molybdenum to expand with the glidcop as it heated. Upon dissecting and examining test pieces under a microscope the braze joints were found to be very good. Numerous other braze tests have been performed with post-brazing examinations to determine the successful methods to use.

The winding of the copper tube around the mandrel was also an area of concern. As the square tube is wound it begins to keystone resulting in a gap larger than can easily be filled in with brazing alloy. Good thermal contact is required between the mandrel and cooling tube so we are currently investigating different methods to fill in the gap. One potential solution is to fill the coil with water then freeze the water. The expansion of the water as it freezes pushes out the outer wall of the coil decreasing the gap. This method has been shown to work well. Another option is to just mechanically press the mandrel groove toward the tubing. A final option is to use a round tube which will not keystone. Any of these options would require more R&D and at this time such work has been halted given the acceptable thermal and vacuum results shown below. Photographs of the prototype construction process and brazing and winding tests can be found on the SLAC LARP Rotatable Collimator website [5].

### 4 ANSYS SIMULATIONS

Extensive simulations have been performed in FLUKA [6] and ANSYS [7] to determine the maximum heating and deflection of the jaws under steady state and transient conditions and are summarized in table 2. “Effective Length” refers to the length of the jaw that is deflected less than  $100\mu\text{m}$  compared to the maximum deflection point – essentially giving the length of the jaw that is still within the beam path under heating conditions. The jaw must then be retracted slightly to meet the 25 micron deflection toward beam spec under steady state. Further simulations were performed to estimate the damage due to the accident scenario. The analysis found an energy deposition of 0.27 MJ in 200 ns with a peak jaw temperature of 57,000 C, sufficient to vaporize the copper. The full extent of the melting is about 5 mm, well within the facet width of 21.54 mm. It is therefore anticipated that the damage will not reach past the exposed facet and rotating the jaw will display a new clean facet to the beam. It was found, however, that this accident case results in a permanent concave deformation of the jaw of 54 microns. This may limit the performance of the collimator after recovering from a collision. The permanent deformation may be partially removed by rotating the jaw by 180 degrees after each hit. The next hit on the other side of the jaw will help remove the deformation caused by the first hit. According to these simulations, the collimator jaw will withstand the beam heating and still function within the specified tolerances. The ultimate test of performance is to place the collimator in an accelerator and test the collimation in real world conditions, however there would be no way to directly

Table 2: Jaw heating and deflection characteristics for Steady State (SS) and Transient (TR) conditions

<b>Component</b>	<b>SS</b>	<b>TR</b>	<b>units</b>
Max jaw temp	70.6	224	C
Max deflection toward beam	105	365	$\mu$ m
Surface Sagitta	226	880	$\mu$ m
Effective length	0.67	0.33	m
Water temp rise	20.3		C
Water pressure drop	2.4		bar

measure the jaw deflection. Bench-top measurements are therefore called for to test the ANSYS predictions for thermal deflections. Unfortunately, there is no way to accurately simulate the beam heating within the jaw without placing the jaw within the path of an actual high energy beam. A substitute must therefore be used. In our case, we chose to use two commercial 5 kW cartridge heaters embedded in the test jaw and illustrated in figures 6 and 7. This setup can approximate the expected steady state heat input of 11.5 kW. To directly compare the bench-top measurements, new ANSYS simulations were performed that accurately represented the heating due to the embedded heaters, accounting for material properties and points of contact between the heaters and the jaw surface. The heaters were embedded in a copper bar which in turn was placed within a slot cut into the jaw surface. Thermal paste was then used to make good thermal contact between the copper bar and jaw and all components were simulated in ANSYS. Water flow was simulated using the model shown in figure 8 which also shows the change in temperature of the water as it passes through the jaw. The overall experimental parameters as simulated in ANSYS, reflecting the real world experimental conditions, are given in table 3

Table 3: Jaw heating and cooling parameters as simulated in ANSYS.

<b>Component</b>	<b>Value</b>	<b>units</b>
Incoming water temp.	20	C
Outgoing water temp.	36.65	C
Water flow	8.3	l/m
water incoming pressure	170	psi
water outgoing pressure	19.5	psi
Heater 1 power	4500	kW
Heater 2 power	4500	kW

The two principle parameters to be measured were the sagitta, or curvature, along the jaw face and the temperature increase. The ANSYS simulation results are given in figure 9. The predicted sagitta is 100 microns and temperature increase is 16.65 C.

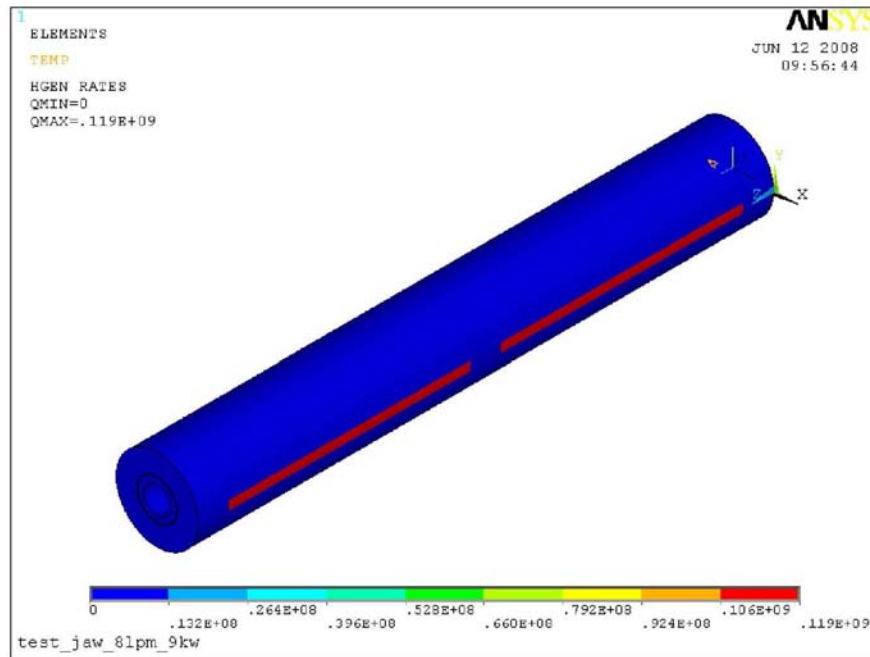


Figure 6: ANSYS output showing the location of the two cartridge heaters embedded in the jaw surface to simulate beam heating.

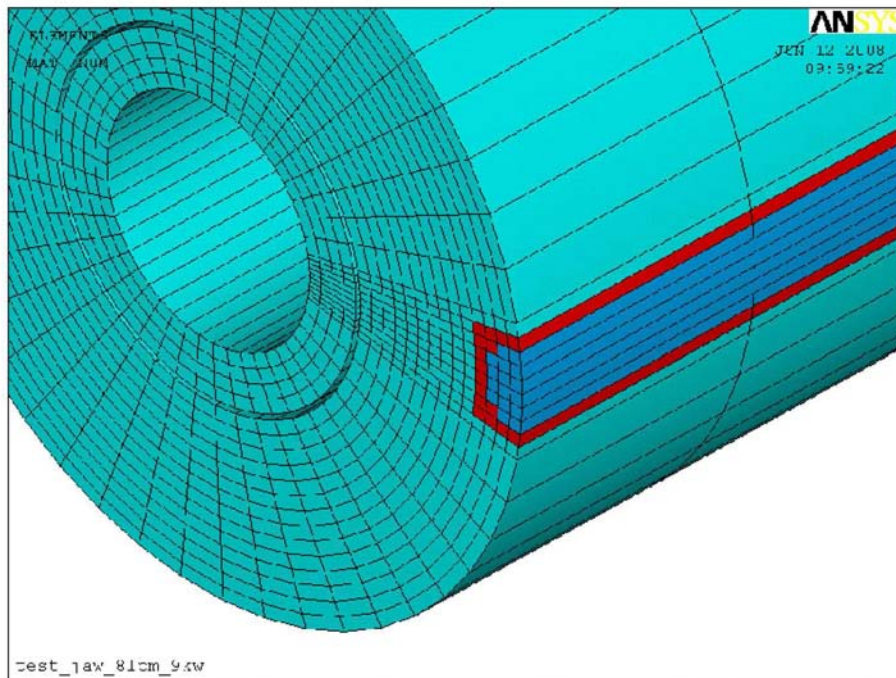


Figure 7: ANSYS output showing the heating rod embedded in a copper bar placed in a slot cut in the jaw surface using thermal paste for contact.



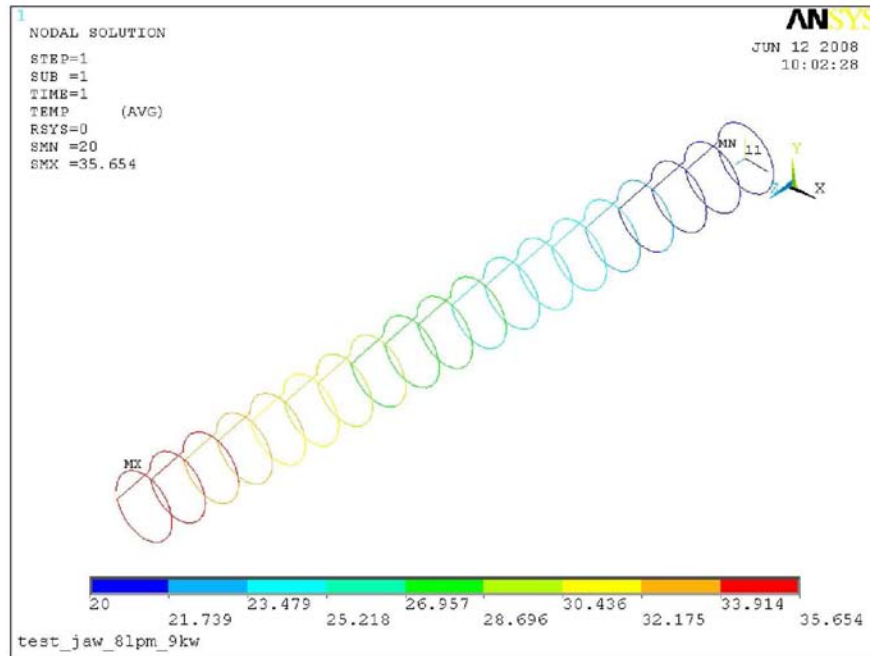


Figure 8: Jaw water flow simulated in the jaw showing water temperature change along jaw.

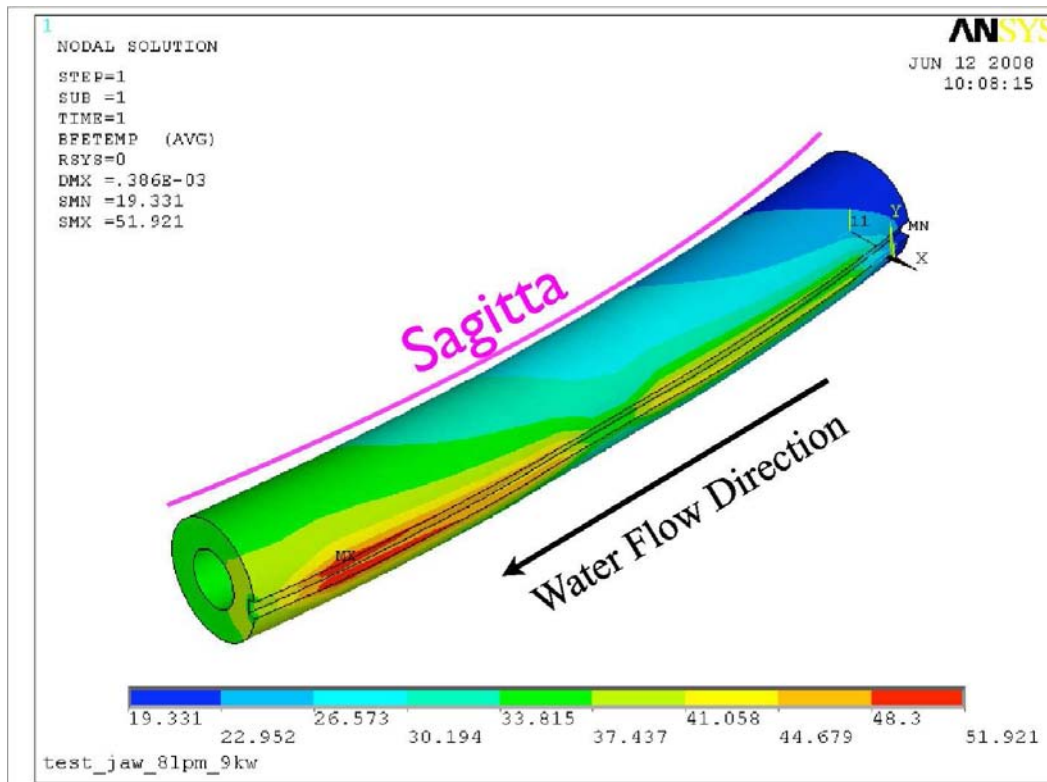


Figure 9: Jaw sagitta and temperature distribution under 9 kW heat load.

## 5 EXPERIMENTAL THERMAL SETUP

The prototype jaw was mounted on the support structure as shown in figure 10. Not shown

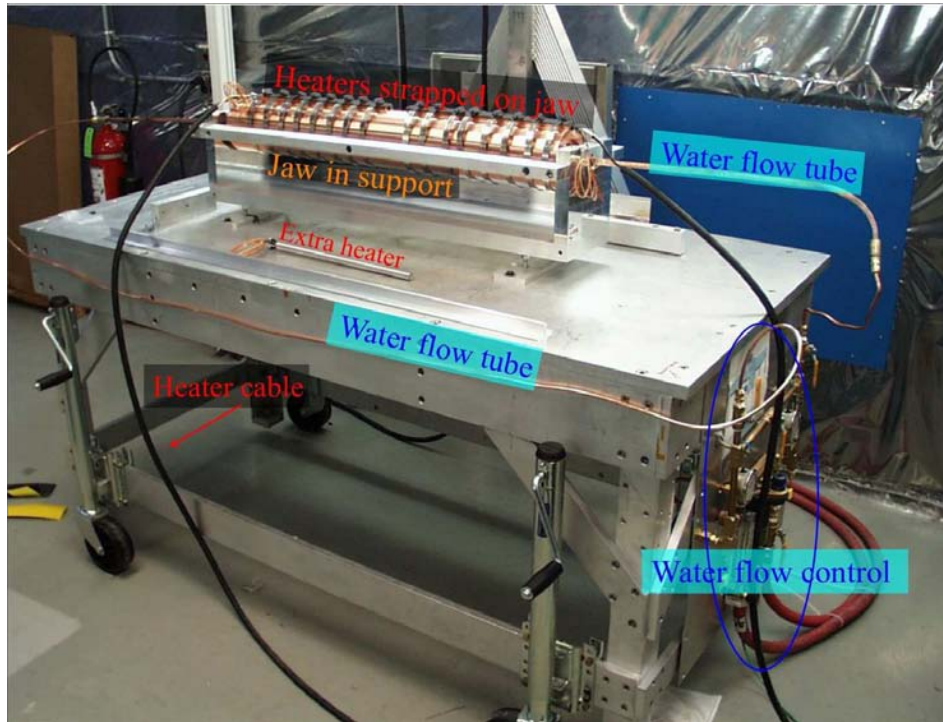


Figure 10: Experimental setup with heaters and cooling attached to jaw prototype.

in the photograph are the two 5 kW heater power supplies and the 16 kW water chiller. The jaw sagitta was measured with three Capacitec [8] HPT-150 capacitive distance sensors which were calibrated for  $\pm 5\mu\text{m}$  accuracy and a precision well within 1 micron. Jaw temperature was monitored using 24 Type K thermocouples with an accuracy of better than  $\pm 1$  F. The mounting of the Capacitec sensors and thermocouples is shown in figure 11. With three Capacitec sensors, one placed at each jaw end and another in the middle, the sagitta can be measured. The jaw is rotatable so sagitta measurements can be performed at any azimuthal angle except near the heaters where the heaters and straps block the view of the Capacitec sensors. In figure 11 the heaters are located on the bottom of the jaw and the Capacitec sensors are measuring the sagitta 180 degrees away from the heaters. The thermocouples were placed longitudinally along the jaw at three azimuthal angles 90, 180 and 270 degrees with respect to the heater location. A total of 27 temperature and Capacitec channels were recorded in real time using a National Instruments Corporation [9] TC-2095 terminal block read by a NI SCXI-1102B amplifier. An extra 7 channels were recorded manually including water flow, water temperature in and out and the power supply voltages and currents. All data was collected using Labview [9].

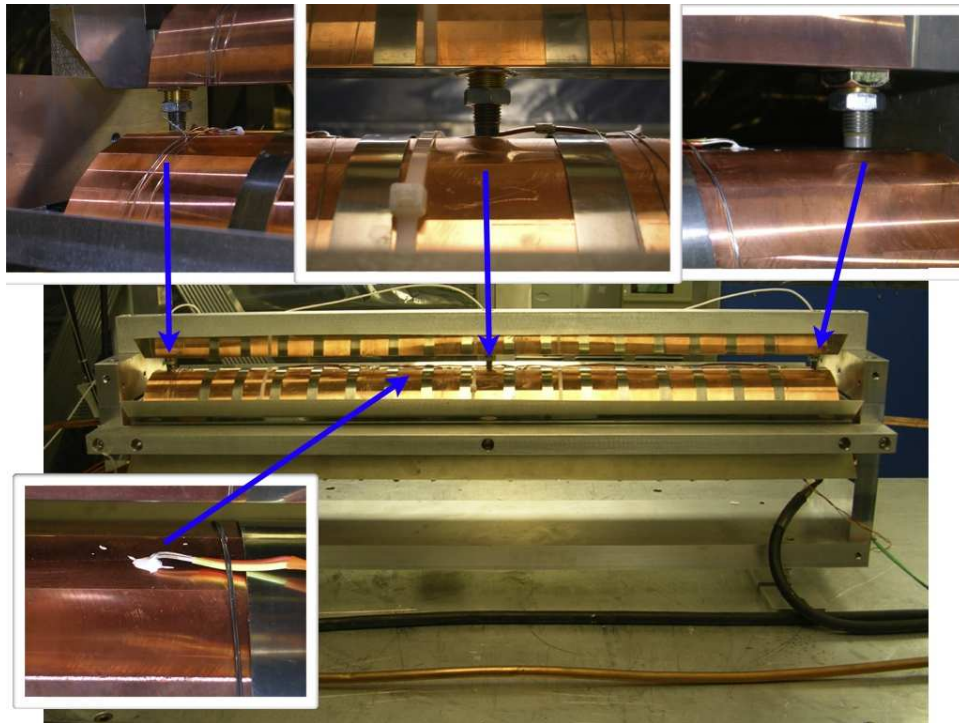


Figure 11: Capacitec Sensors mounted on Jaw support. Shown are zooms onto the location of each sensor plus one thermocouple. Also shown are the heat deflectors used to keep the support bars cool.

## 6 EXPERIMENTAL THERMAL RESULTS

A subset of the raw data is shown in figures 12, 13 and 14. From the current and voltage

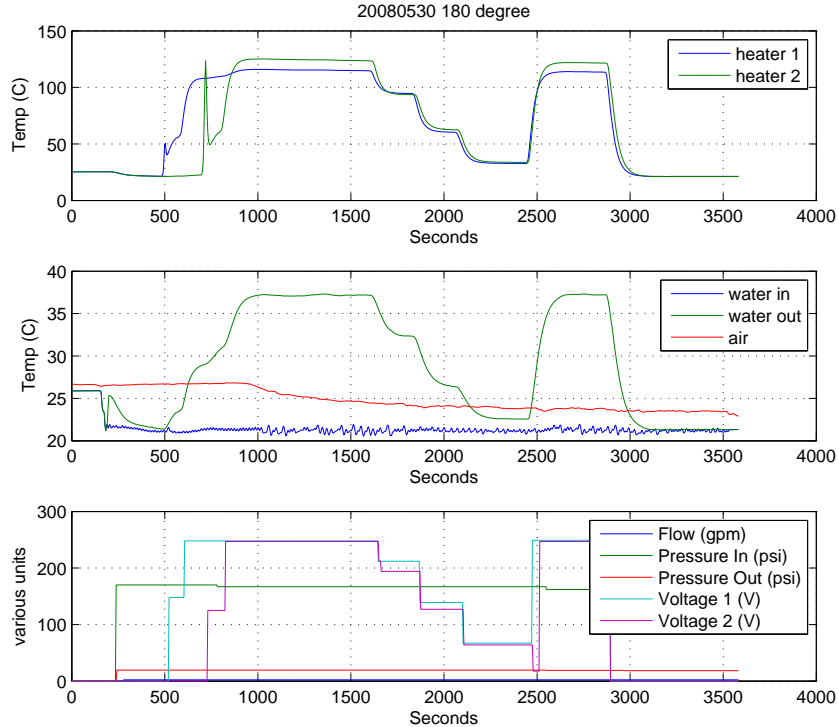


Figure 12: Recorded heater current and temperature, water flow and temperature and air temperature.

From the power supplies data shown in figure 12 it can be calculated that the heater block supplies  $9006 \pm 235$  Watts to the jaw. From the water flow and temperature change it can be calculated that the energy absorbed in the water is  $9322 \pm 710$  Watts. This means that little of the heat is dissipated through the air or by radiation; the heat flow is from the heaters and through the water. The setup therefore realistically simulates the environment of a beam heated jaw in the LHC vacuum chamber.

The measured sagitta at six azimuthal locations around the jaw are shown compared to the ANSYS predicted curve in figure 15. The thermocouple readings compared to the ANSYS predictions are shown in figure 16. As can be seen, the measured sagitta at 180 degrees is slightly greater than expected at 112 microns. The temperature along the jaw is also consistently about 3 degrees higher than the ANSYS results. One source of discrepancy is the actual incoming water temperature was about 21.5 C whereas the ANSYS model used 20 C. This can account for about half the temperature disagreement and brings the results in close agreement. The sagitta measurement disagreement of 12% is small and gives us confidence that our ANSYS simulations are accurately giving the jaw deformation due to realistic beam heating.

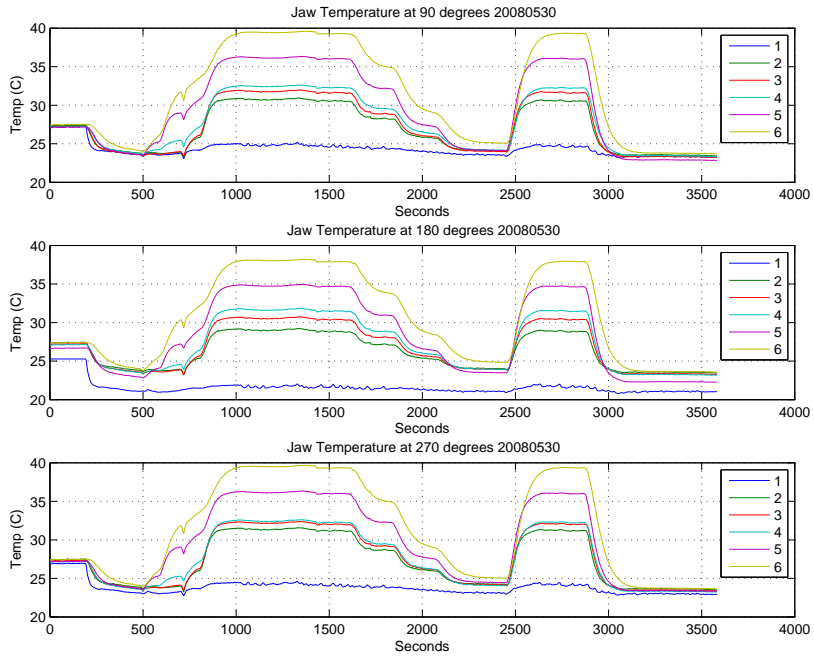


Figure 13: Recorded temperatures along jaw at three different azimuthal angles.

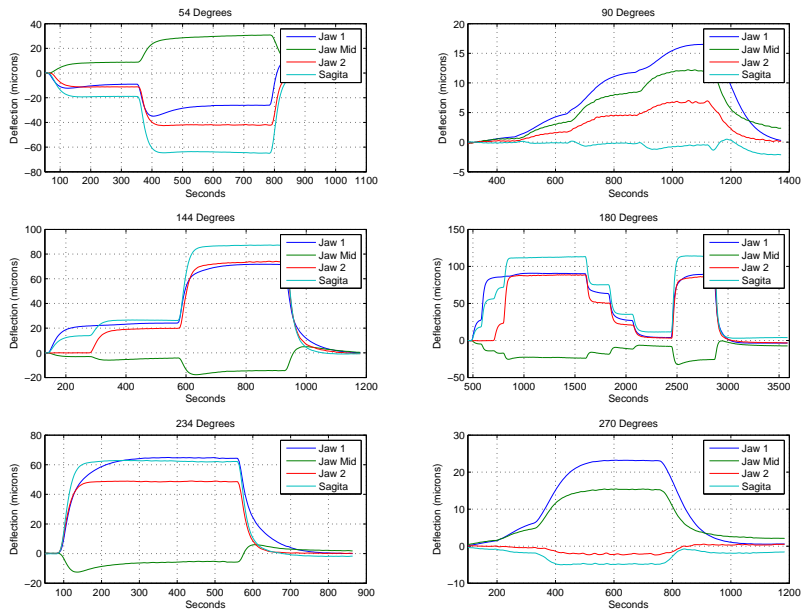


Figure 14: Capacitec measurements and calculated sagitta at six different azimuthal angles around the jaw.

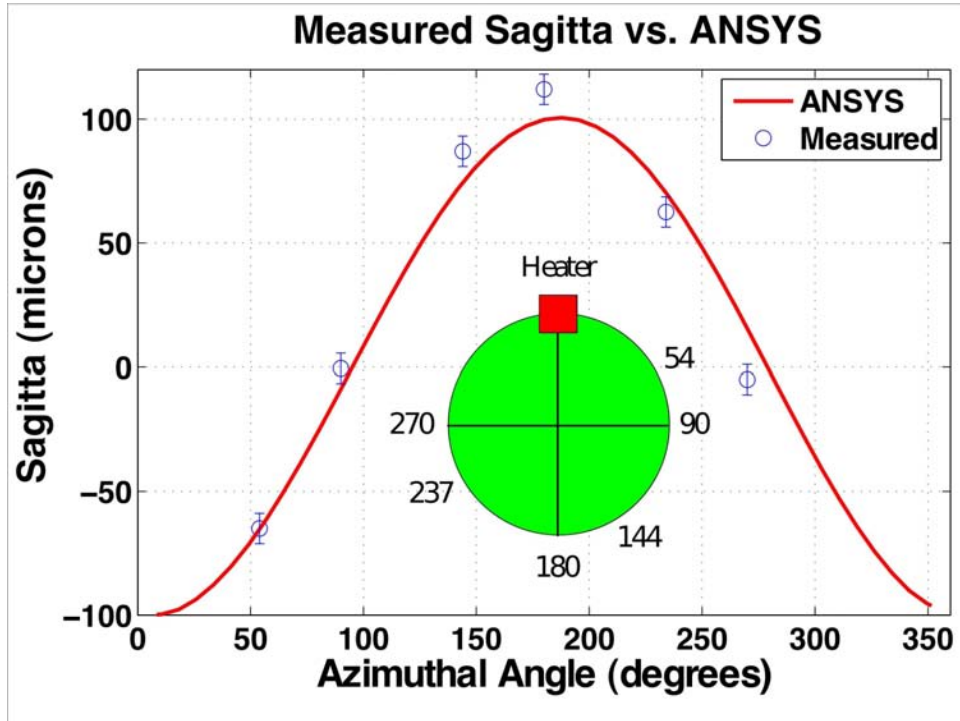


Figure 15: Measured sagitta at six azimuthal location compared to the ANSYS curve,.

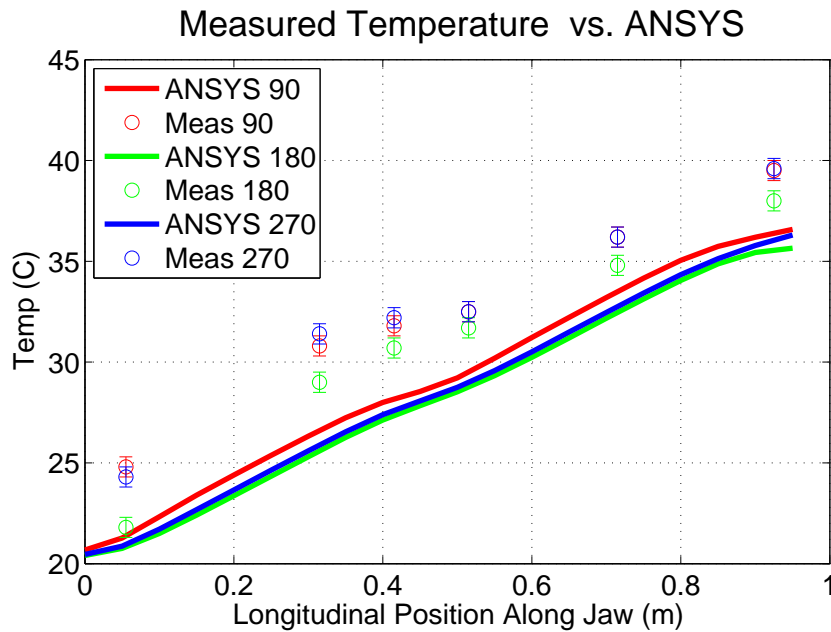


Figure 16: Measured temperature along the jaw at three azimuthal locations compared to the ANSYS predictions.

There was concern that the support bars holding in the jaw and sensors would deform as they were heated. ANSYS simulations showed that the aluminum bars would have had to have a temperature variation along their heights of about 1 F for there to be a deformation

on the order of 10 microns. Thermocouples were placed along the support bars as well to verify the temperature gradient was well under 1 degree. Radiant heat deflectors were also placed along each bar as shown in figure 11 to help deflect the heat away from the bars. With these measurements and precautions we believe the sagitta measurements accurately measure the deformation of the jaw and not the support stand.

## 7 VACUUM BAKE-OUT TESTS

The jaw was placed in a custom built vacuum chamber to determine if the target vacuum pressure could be achieved. The jaw was first hydrogen fired in a brazing furnace at 850C before bake-out to help clean all surfaces after a large amount of handling during the thermal tests and to accelerate the bake-out process. The standard PEP-II Beamline bake-out sequence [10] was then used to characterize the vacuum quality. It was inserted into the vacuum vessel and baked at varying temperatures for a total of 14 days. The chamber temperature and resultant pressure over this time is plotted in figure 17. The final measured

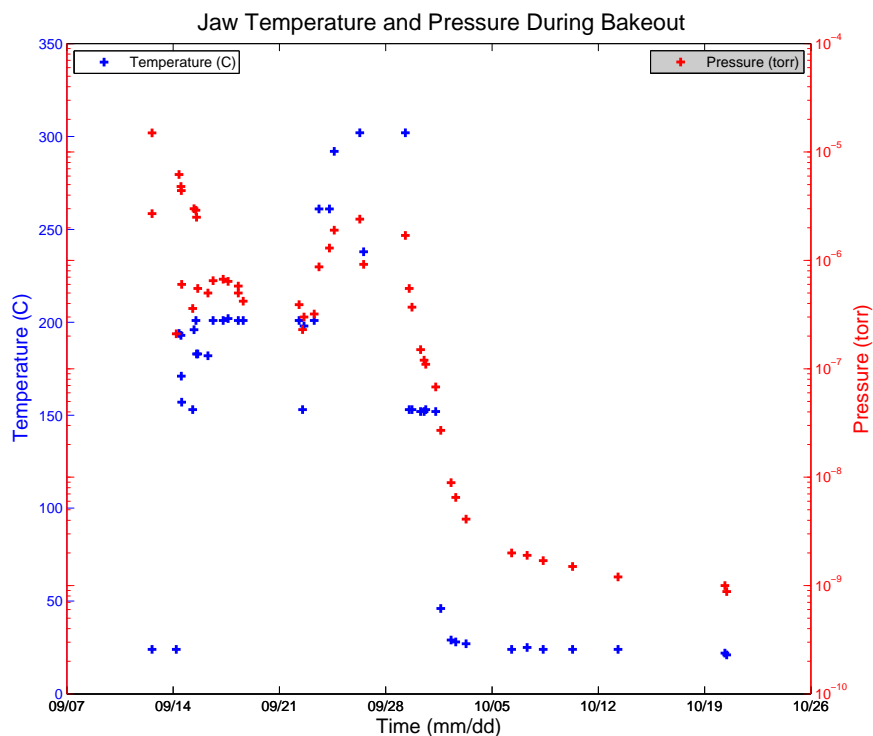


Figure 17: Jaw vacuum pressure during bakeout.

pressure was  $8.8 \times 10^{-10}$  Torr after several days of cool-down but had not yet fully bottomed out. After a shorter bake-out period the vacuum chamber without the jaw present obtained a pressure of  $2.0 \times 10^{-9}$  Torr. With a longer bake-out and pumping time it is expected the empty chamber would have obtained a much better vacuum and so the fractional part of the pressure due solely to the jaw cannot be determined.

The LHC vacuum spec is  $7.5 \times 10^{-10}$  Torr [3]. It can be difficult to directly compare partial vacuums in two different systems with different pump configurations. The ion pumps used in the bake-out test had a pumping speed of 400 l/s which is similar to the expected pumping rate of the collimator chamber installed in the LHC beam pipe [11] so some comparisons can be made. Expecting the internal surface area of the bake-out vacuum chamber to be similar to the full collimator chamber and that we will have a total of two jaws in the chamber and the pumping speed is similar, our estimated full collimator pressure is to be around  $1 \times 10^{-9}$  Torr. This is slightly above spec but close. A longer bake-out time may be adequate to reach the spec. It should also be noted that the phase I graphite collimators currently installed in the LHC were never able to reach the  $7.5 \times 10^{-10}$  Torr spec. These devices were granted a higher pressure spec of  $3.8 \times 10^{-8}$  Torr [12]. This laxer spec can be easily reached by our device but we anticipate achieving the tighter spec as well. A lower pressure in our design is not surprising considering the lack of graphite which has a long outgasing period.

An RGA scan was performed near the end of the run with results in figure 18. The main potential concern would be the presence of any hydrocarbons which cannot be present in the LHC vacuum. As can be seen, there are no detected molecules larger than carbon dioxide (mass = 39). All efforts were taken to minimize the RCO's exposure to hydrocarbons by using only alcohol as the cutting fluid and maintaining clean working environments. Our efforts were a clear success.

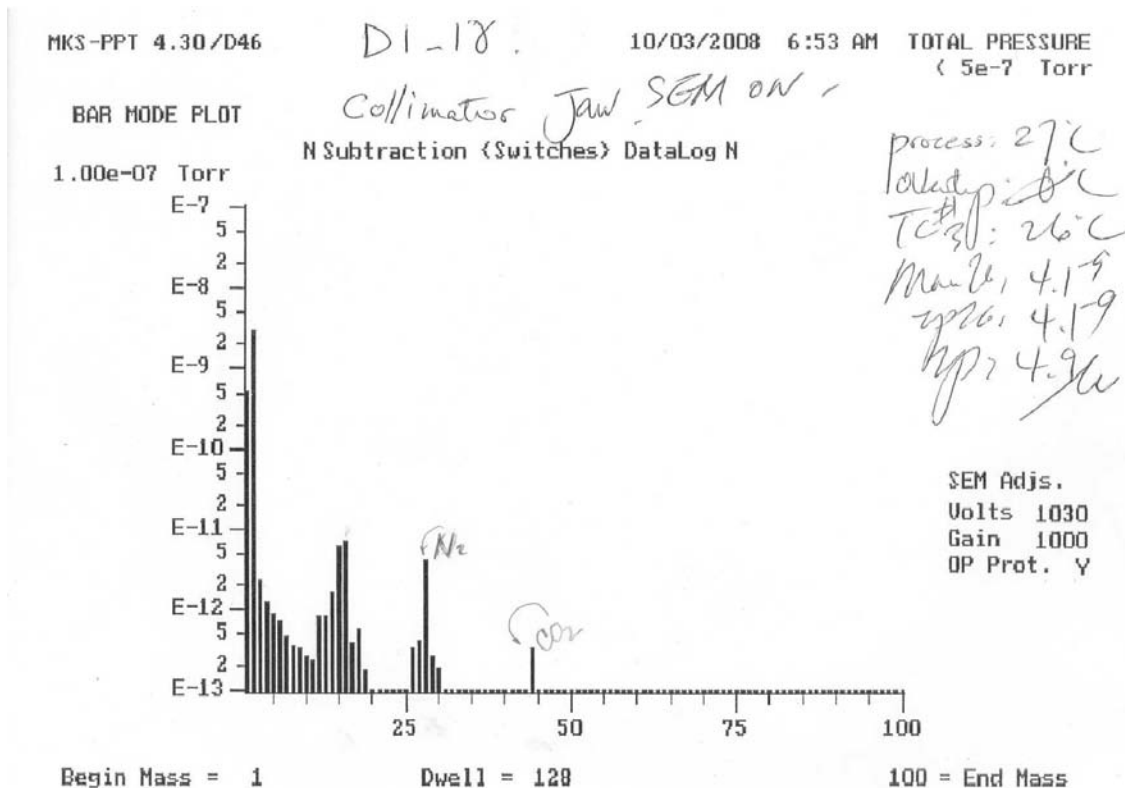


Figure 18: RGA scan of jaw at end of vacuum tests



facet	max negative deviation (mil)	max positive deviation (mil)	total deviation (mil)
1	-0.6	1.0	1.7
5	-0.5	0.7	1.3
8	-0.5	0.5	1.0
13	-0.7	0.6	1.3
16	-0.5	0.8	1.3

Table 4: Summary of RC0 CMM survey after vacuum test.

## 8 FLATNESS MEASUREMENTS

Directly after the machining of the jaw facets and while the jaw was still in the mill a dial indicator gauge was used to confirm the flatness of each facet was within 1 mil. No more detailed flatness measurements were performed at that time.

After all thermal and vacuum tests the RC0 jaw was placed in a CMM to measure the flatness of the jaw facets. 5 nonconsecutive facets were measured for overall flatness with three survey lines per facet totaling 99 points per facet. To account for the edge taper that will exist on the final jaw but not machined into this prototype, the survey points began 3.5 cm from the edge of the jaw. The survey results are summarized in table 4. The overall shape of each facet is roughly the same and so the details will only be shown for facet #1 in figures 19, 20, 21 and 22. This is the worst (least flat) measured facet and gives a lower bound to the flatness. The shape is bowing where the outer edges bow out and the center bows in to form a concave shape. Overall, the flatness is slightly above the spec of 1 mil (or 25 microns).

Several factors contributed to the overall shape and a lot can be attributed to the facet machining method. The support for the facet in the milling machine was not as well aligned as possible and due to potential off center indexing and misalignment of the milling head with respect to the mill table and jaw the facets were probably not machined purely square. The jaw was supported by the ends of the molybdenum central shaft. Gravity and the force of the mill head on the part probably contributed to the overall bowed shape. It should also be noted that this prototype jaw experienced severe trauma while brazing. During one cycle, too much braze material was used and the molybdenum shaft was accidentally brazed to the brazing oven. This caused the end of the shaft and mandrel to be severely bent. The shaft and mandrel was successfully pried back into shape well enough for the thermal tests to continue but not to mil precision. The facet machining method was performed after this accident and most likely resulted in the molybdenum shaft no longer being concentric inside the jaw. This in turn will have resulted in non-concentric indexing and an overall conic shape to the jaw surface. No such accident will be acceptable for the final jaws and this will eliminate much of the warpage of the jaw facets.

Since the bowing of the jaw is azimuthally symmetric about the jaw (i.e. each facet has the same overall shape) it is concluded that none of the deformed shape of the jaw was due to the vacuum bake-out. Movement due to overheating would have caused asymmetrical warping. In order for the shape shown in the survey to occur due to heating, the total amount of copper material would have had to have changed. This is impossible simply

by applying heat (if below melting temperatures). Instead, the shape must be due to the machining method. It is expected that an improved machining method will remove most of the error in flatness. Also, in the final manufacturing process the 850C bake-out will not occur, eliminating even the possibility that this will contribute to the non-flatness of the facets.

In summary, the RC0 facets are close to the flatness specification. This is in spite of several factors that contributed to non-ideal facet machining. It is fully anticipated that an improved machining method will meet the specification.

## 9 ACKNOWLEDGMENTS

Special thanks goes to Doug McCormick for helping in setting up the NI equipment. Thanks also goes to the techs in Building 33 for their help in the experimental setup. The SLAC klystron department has extensive experience in brazing techniques and has helped us greatly in our endeavors.

## References

- [1] Lari, L., "Evaluation of Beam Loss and Energy Deposition for One Possible Phase II Design for LHC Collimation," Proceedings EPAC08 **WEPP072** (2008)
- [2] LHC Design Report, CERN-entire 2004-003 (2004)
- [3] Cai, Y *et al.*, "LHC Phase II Rotary Consumable Collimator - RC1 Conceptual Design Report," Rev 2, (2005)
- [4] Smith, J.C. *et al.*, "Bench-top Impedance Measurements for a Rotatable Copper Collimator for the LHC Phase II Collimation Upgrade," EPAC08 **MOPC095** (2008)
- [5] <http://www-project.slac.stanford.edu/ilc/larp/rc/default.htm>
- [6] [www.fluka.org](http://www.fluka.org)
- [7] [www.ansys.com](http://www.ansys.com)
- [8] [www.capacitec.com](http://www.capacitec.com)
- [9] [www.ni.com](http://www.ni.com)
- [10] SLAC MFD Vacuum Group, "Vacuum Department Guidelines for Vacuum Systems," SLAC-I-007-12004-001 R1 (2003)
- [11] Wevers, Ivo, CERN TS/MME dept., private communication
- [12] Aberle, Oliver, CERN AB/ATB dept., private communication

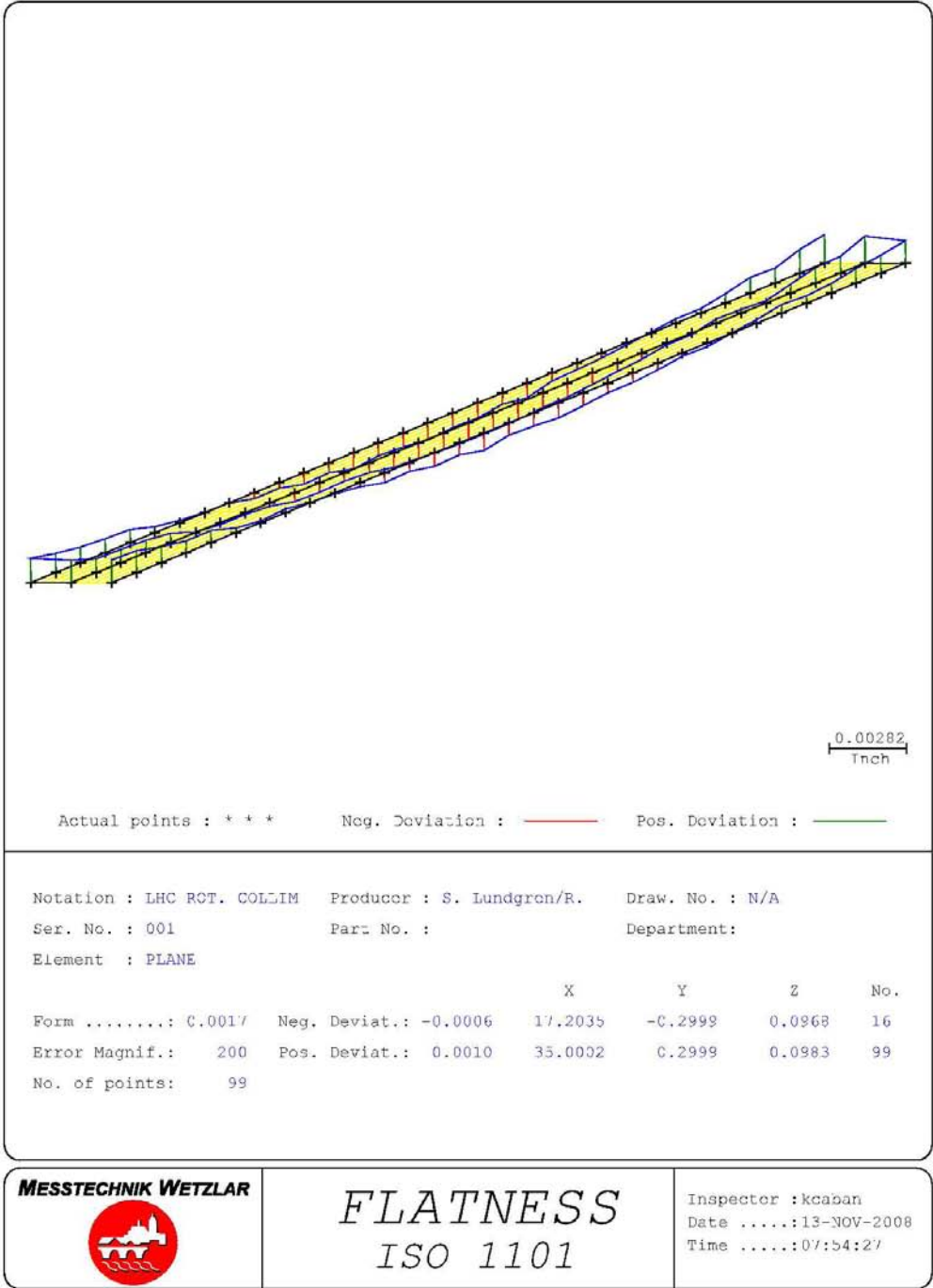


Figure 19: CMM survey summary for Facet # 1.

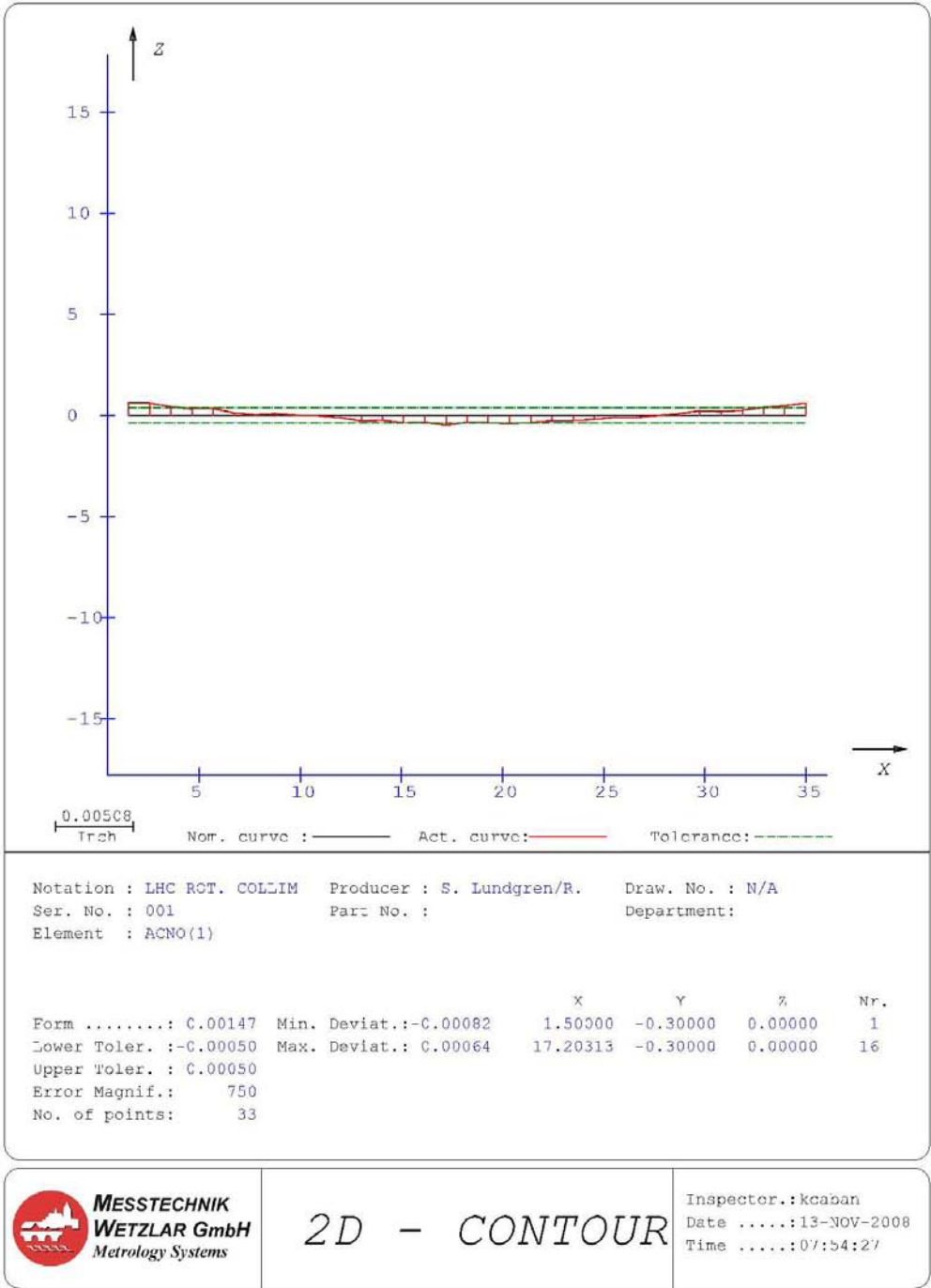


Figure 20: CMM survey results part 1 for Facet # 1.

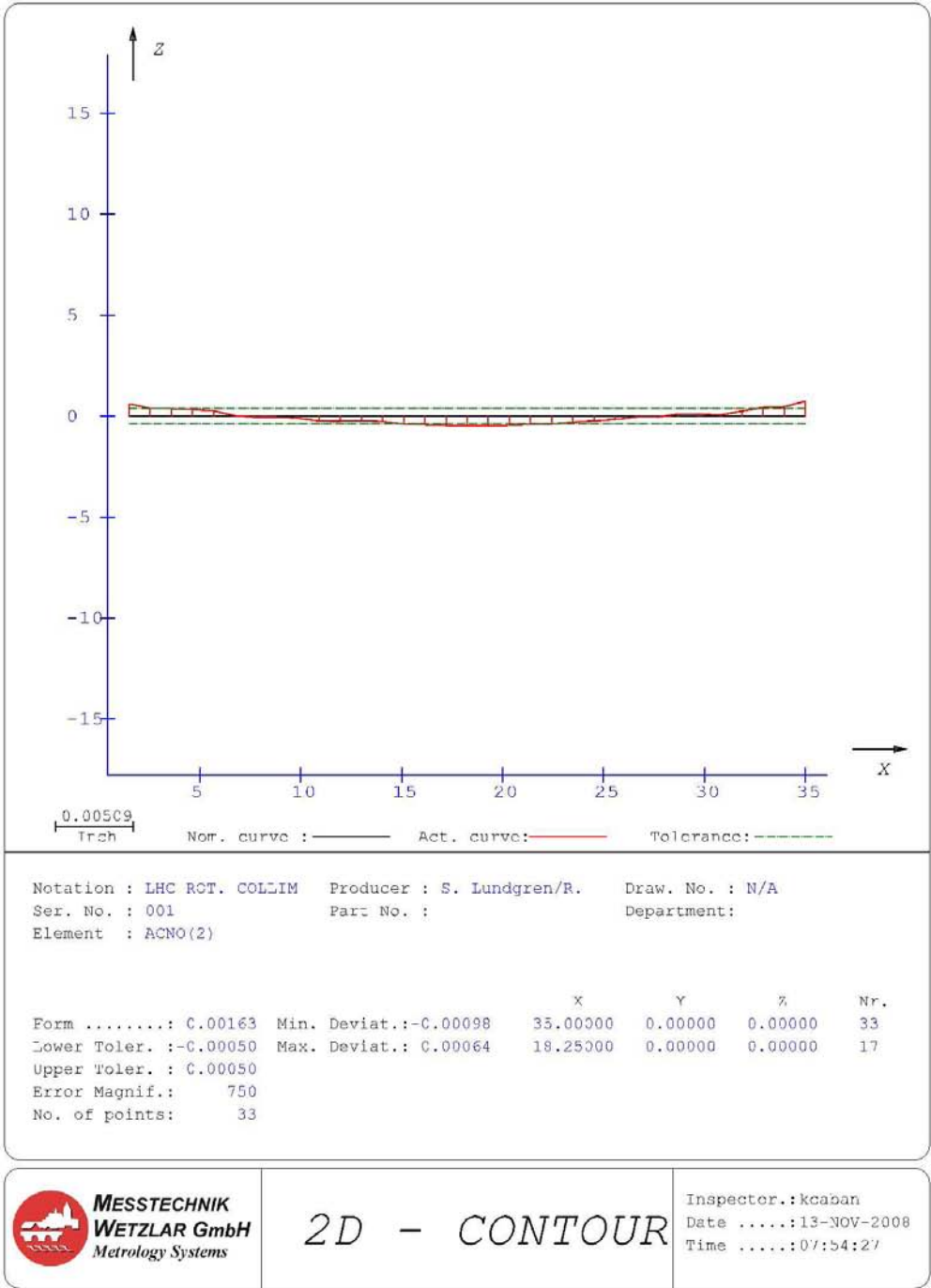


Figure 21: CMM survey results part 2 for Facet # 1.

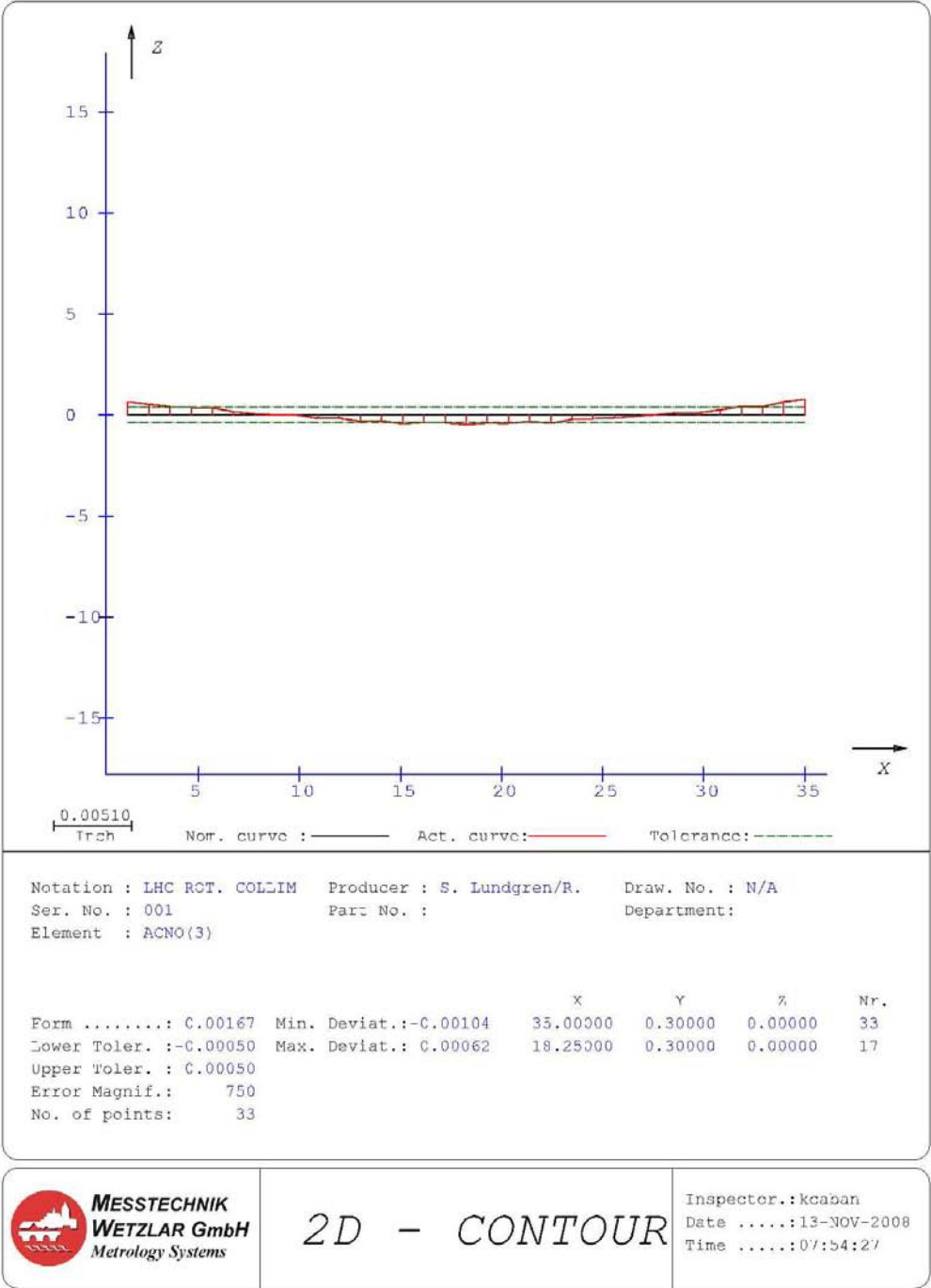


Figure 22: CMM survey results part 3 for Facet # 1.